Molecular Biology of the Cell
Vol. 11, 3911–3923, November 2000

Nidogen Is Nonessential and Not Required for Normal Type IV Collagen Localization in *Caenorhabditis elegans*

Seong Hoon Kang and James M. Kramer*

Department of Cell and Molecular Biology, Northwestern University Medical School, Chicago, Illinois 60611

Submitted May 24, 2000; Revised August 21, 2000; Accepted September 15, 2000
Monitoring Editor: Judith Kimble

Nidogen (entactin) can form a ternary complex with type IV collagen and laminin and is thought to play a critical role in basement membrane assembly. We show that the *Caenorhabditis elegans* nidogen homologue *nid-1* generates three isoforms that differ in numbers of rod domain endothelial growth factor repeats and are differentially expressed during development. NID-1 appears at the start of embryonic morphogenesis associated with muscle cells and subsequently accumulates on pharyngeal, intestinal, and gonad primordia. In larvae and adults NID-1 is detected in most basement membranes but accumulates most strongly around the nerve ring and developing gonad. NID-1 is concentrated under dense bodies, at the edges of muscle quadrants, and on the sublateral nerves that run under muscles. Two deletions in *nid-1* were isolated: *cg119* is a molecular null, whereas *cg118* produces truncated NID-1 missing the G2 collagen IV binding domain. Neither deletion causes overt abnormal phenotypes, except for mildly reduced fecundity. Truncated *cg118* NID-1 shows wild-type localization, demonstrating that the G2 domain is not necessary for nidogen assembly. Both *nid-1* mutants assemble type IV collagen in a completely wild-type pattern, demonstrating that nidogen is not essential for type IV collagen assembly into basement membranes.

INTRODUCTION

Basement membranes are thin extracellular matrices that have important roles in the development and functions of many tissues. The major constituents of basement membranes include type IV collagens, laminins, nidogen (entactin), and proteoglycans. Interactions between these constituents and their interactions with cell surface molecules are critical for the assembly and function of basement membranes (Yurchenco, 1994; Timpl, 1996). Collagen IV and laminin can independently polymerize in a concentration-dependent manner to form separate networks in the basement membrane (Yurchenco and Furthmayr, 1984; Yurchenco *et al.*, 1992; Yurchenco and Cheng, 1993). Connection between these independent networks is thought to be mediated by nidogen, which can bind both collagen IV and laminin with high affinity (Fox *et al.*, 1991).

Nidogen is a 150-kDa glycoprotein that consists of two amino (G1, G2) and one carboxyl (G3) terminal globular domains that are connected by a rod domain composed primarily of endothelial growth factor (EGF) repeats (Durkin *et al.*, 1988; Mann *et al.*, 1989; Fox *et al.*, 1991). Mammals express two closely related forms of nidogen, nidogen-1 and nidogen-2, that are encoded by separate genes (Kohfeldt *et al.*, 1998). Both nidogen-1 and nidogen-2 bind type IV collagen, perlecan, and laminin with high affinity (Aumailley *et al.*, 1993; Chung *et al.*, 1993; Kohfeldt *et al.*, 1998). The G3 domain of nidogen-1 binds strongly to a single EGF module in the laminin γ1 chain (Mayer *et al.*, 1993), whereas nidogen-2 shows strong interaction with LG domains of the laminin α2 chain (Kohfeldt *et al.*, 1998; Talts *et al.*, 1999). Binding of nidogen-1 to collagen IV and perlecan occurs through the nidogen G2 domain (Reinhardt *et al.*, 1993). Using purified proteins, nidogen-1 was shown to form a ternary complex with type IV collagen and laminin-1 (Aumailley *et al.*, 1993). The ability of nidogen to bind both the collagen IV and laminin networks with high affinity suggests that this linking function may be critical for basement membrane assembly.

Several lines of evidence suggest that nidogen-1 has important functions in vertebrate development and differentiation. Nidogen-1 promotes attachment of cells in culture, mediated through the single RGD sequence within its rod domain and by sequences in the G2 domain (Yelian *et al.*, 1993; Dong *et al.*, 1995; Wu *et al.*, 1995). Addition of antibodies that interfere with nidogen-1 binding to laminin disrupts epithelial morphogenesis of cultured embryonic kidney,

* Corresponding author. E-mail address: jkramer@nwu.edu.

lung, or submandibular glands (Ekblom *et al.*, 1994; Kadoya *et al.*, 1997). Nidogen proteolysis has been correlated with loss of epithelial function during normal mammary gland involution and during gland regression induced by ectopic stromelysin-1 expression (Alexander *et al.*, 1996). Nidogen-1 can cooperate with laminin-1 to stimulate β-casein synthesis by cultured mammary epithelial cells (Pujuguet *et al.*, 2000). These studies suggest that nidogen may have critical developmental functions in vivo.

To examine the in vivo functions of nidogen, we initiated studies of its roles in *Caenorhabditis elegans* development. Several basement membrane components have been shown to be essential for embryonic development in *C. elegans* (Kramer, 1997). Loss or alteration of type IV collagen (Guo *et al.*, 1991; Sibley *et al.*, 1993; Gupta *et al.*, 1997), perlecan (Rogalski *et al.*, 1993), or SPARC/osteonectin (Fitzgerald and Schwarzbauer, 1998) result in arrest during the mid to late stages of embryogenesis. Mutations in other basement membrane components that are required for the proper assembly of collagen IV, perlecan, or SPARC might be expected to also result in defective development.

The mechanisms of assembly of these molecules into basement membranes may differ. Perlecan is expressed in muscle cells and assembles into the basement membranes immediately adjacent to the cells that synthesize it (Moerman *et al.*, 1996). In contrast, type IV collagen (Graham *et al.*, 1997) and SPARC (Fitzgerald and Schwarzbauer, 1998) assemble into basement membranes associated with tissues that do not express the proteins. Epitope-tagged type IV collagen synthesized in body wall muscle cells can assemble into basement membranes that surround the pharynx, intestine, and gonad. Expression only in muscle cells was also shown to be sufficient to rescue the lethality of a type IV collagen null mutant and to provide modest fertility (Graham *et al.*, 1997). In addition, type IV collagen is localized to certain basement membranes in *C. elegans* and absent from others, even though all are open to the pseudocoelom, which is the source of free collagen IV molecules. These studies indicated that a mechanism for directing type IV collagen assembly to particular locations must exist.

Laminin appears earlier than type IV collagen during mouse (Leivo *et al.*, 1980; Dziadek and Timpl, 1985) and *Drosophila* development (Kuschegullberg *et al.*, 1992) and during formation of new basement membranes in angiogenesis (Form *et al.*, 1986). In a coculture of epithelial and mesenchymal cells, antisense inhibition of laminin expression blocked deposition of type IV collagen and nidogen at the cellular interface, indicating the importance of laminin for basement membrane assembly (De Arcangelis *et al.*, 1996). Because nidogen can serve as a link between type IV collagen and laminin, it is possible that collagen IV could be localized by binding to nidogen that is associated with laminin already present at tissue surfaces. Thus, the earlier localized laminin could provide a pericellular binding site to concentrate collagen IV and allow its assembly. Nidogen would be required to meditate this interaction because collagen IV and laminin have not been found to directly interact.

To determine what roles nidogen might play in *C. elegans* development and whether it is involved in localization of type IV collagen assembly, we generated mutations in the *C. elegans* nidogen gene. Here we present characterization of the *C. elegans* nidogen gene *nid-1* and analysis of mutations in it.

MATERIALS AND METHODS

Characterization of the nid-1 Gene

A *C. elegans* nidogen homologue was identified in the cosmid F54F3 (GenBank Z79696). All numbering presented is based on this GenBank sequence. Sequence and restriction analyses of RT-PCR products derived from predicted exons and six existing cDNA clones identified three alternative splice variants of the *nid-1* gene. Three of the cDNAs (yk38f9, yk64d8, yk152d12) contain all exons and encode NID-1 form A, one (yk7a9) is missing exon 11 and encodes form B, and two (yk33c12, yk161f6) are missing exons 11–14 and encode form C. All other predicted intron/exon boundaries were confirmed by sequence analyses of these clones.

nid-1 Mutations

Animals were maintained as described by Brenner (Brenner, 1974). Isolation of *nid-1* mutations generally followed previously described methods (Plasterk, 1995). A transposon Tc1 insertion allele of *nid-1, ev608::Tc1*, was identified from a library of animals carrying *mut-2(r459)*. The Tc1 insertion site was localized to between nucleotides 3041–3042 by sequence analysis. Tc1 excision deletion alleles were identified by PCR screening populations of *mut-2(r459); nid-1(ev608::Tc1)* animals using primers flanking the Tc1 insertion site. Homozygous *cg118* and *cg119* deletion mutant animals were isolated by sib-selection. The extents of the deletions were determined by sequencing PCR-generated clones spanning the deletions. All mutations were outcrossed a minimum of seven times before further analyses.

Production of Anti-NID-1 Antiserum

A GST-NID-1 fusion construct was generated by cloning the 1.3-kb *Nci*I-*Xho*I (nucleotides 7820–9521 genomic) fragment from the cDNA yk38f9 (D36924, D33953) into the pGEX-4T1 (Pharmacia Biotechnology, Piscataway, NJ) vector. This construct expresses the last 22 amino acids of the rod domain and the complete G3 domain of NID-1 fused to the carboxyl end of GST. The fusion protein was SDS-PAGE purified and used to immunize rabbits. An MBP-NID-1(G3 domain) fusion protein was generated by inserting the 1.1-kb *Pvu*II-*Xho*I fragment (nucleotides 8239–9521) from the yk38f9 cDNA into the pMAL-c2 vector (New England Biolabs, Beverly, MA). The purified pMAL fusion protein was used to affinity purify the rabbit antisera as previously described (Graham *et al.*, 1997).

Western Blot Analyses

Embryos or mixed stage animals were quick-frozen in liquid nitrogen, pulverized while frozen, and extracted with 6 M guanidine-HCl, 50 mM Tris-HCl (pH 7.4), containing 10 mM EDTA, 2 mM *N*-ethylmaleimide (NEM), and 2 mM PMSF (Dziadek and Timpl, 1985). Guanidine extracts were dialyzed against 7 M urea, 50 mM Tris-HCl (pH 8.6) with 10 mM EDTA, 5 mM NEM, and 5 mM PMSF at 4°C. The resulting supernatants were acetone precipitated and resuspended in dH_2O. Samples were subjected to 7% SDS-PAGE and transferred to nitrocellulose filters. Filters were reacted with affinity purified anti–NID-1 antiserum diluted 1:500 and detected using the ECL system (Amersham Pharmacia Biotechnology).

Immunocytochemistry

Embryos were purified by alkaline hypochlorite treatment and fixed with 4% paraformaldehyde as described previously (Graham *et al.*, 1997). Larval and adult animals were prepared as described (Finney and Ruvkun, 1990). After fixation, samples were rehydrated and

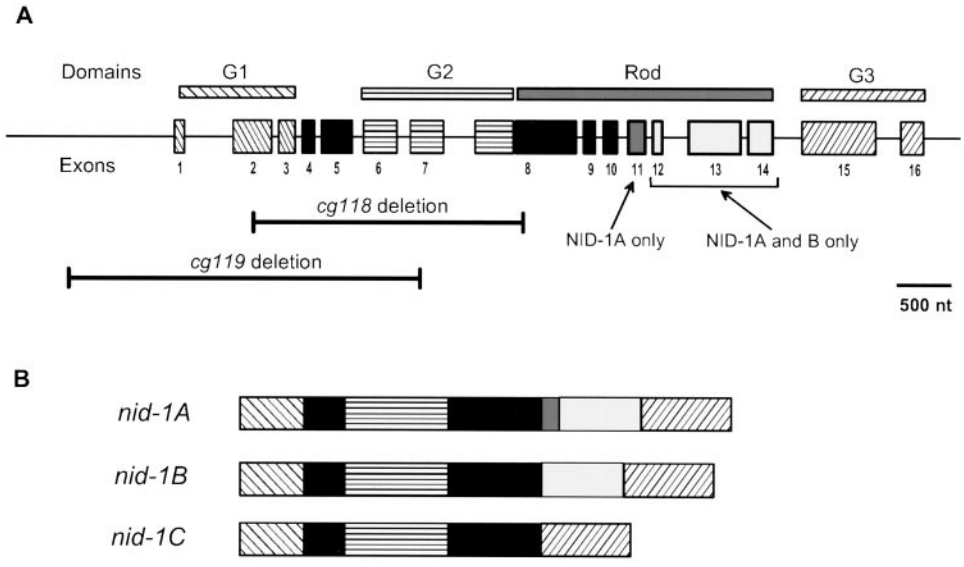

Figure 1. Structure of the *C. elegans* nid-1 nidogen gene. (A) Exons are indicated as boxes with numbers below. The *nid-1A*-specific exon 11 is colored dark gray, and the *nid-1A*– and *B*–specific exons 12–14 are colored light gray. The extents of the G1, G2, and G3 globular domains and the rod domain are indicated at the top of the figure. The extents of the *cg118* and *cg119* deletions are shown below the figure. (B) The structures of the three alternatively spliced transcripts generated from the *nid-1* gene.

blocked for 1 h in PBS containing 0.1% Triton X-100 (PBS-T) and 10% normal donkey serum (NDS). Samples were then incubated overnight at room temperature with various primary antibodies diluted with PBS-T-NDS: anti–NID-1 (1:50), anti–LET-2 type IV collagen (1:100) (Graham *et al.*, 1997), monoclonal anti–MHC-A myosin (1:1000), MH35 anti–α-actinin (1:500) (Francis and Waterston, 1985). Samples were washed three times with PBS-T, incubated for 1 h at room temperature with FITC-labeled donkey anti-rabbit and Texas red-labeled donkey anti-mouse secondary antibodies (Jackson ImmunoResearch, West Grove, PA) in PBS-T-NDS, and washed with PBS-T and PBS. All samples were mounted with 90% glycerol in PBS (pH 8.0) containing 1 mg/ml para-phenylenediamine and 1% DABCO. Images were captured on ASA 400 color slide film or digitally recorded with a digital camera. Digital images were deconvolved (VayTek, Inc., Fairfield, IA) to remove out-of-focus information, and contrast and brightness were adjusted using Adobe Photoshop (San Jose, CA).

nid-1 Expression Analyses

RNA was extracted from *C. elegans* samples using TRIZOL reagent (Life Technologies-BRL, Grand Island, NY). Poly-A–enriched RNA was isolated using batch oligo(dT)-cellulose chromatography (Sambrook *et al.*, 1989). Six-microgram samples of poly-A–enriched RNA were fractioned on 0.8% formaldehyde-agarose gels and transferred to nylon membranes. The membranes were hybridized to ^{32}P-labeled *nid-1* exon 11–, exon 13–, or exon 15–specific probes in modified Church buffer (50% formamide, 250 mM NaCl, 250 mM Na_2PO_4, 6% SDS, and 6% polyethylene glycol) and washed with 2× SSC, 0.1% SDS at 37°C for 45 min and with 0.2× SSC, 0.1% SDS at 60°C for 30 min.

nid-1 Phenotypic Analyses

Organization of epidermal cells was examined in *jcIs1; cg118* and *jcIs1; cg119* animals. *jcIs1* expresses the JAM-1::GFP marker, which labels adherens junctions between cells (Mohler *et al.*, 1998). The presence of *cg118* or *cg119* were confirmed by PCR analysis for the corresponding deletion. The morphologies of excretory cells and gonads were determined by observations of live *nid-1* mutant animals using Nomarski DIC optics.

To determine fecundity, individual animals were picked at the L4 larval stage and were transferred daily to new plates until they stopped laying fertilized eggs. The total numbers of eggs laid each day was counted using a dissecting microscope. For the reported analysis animals were maintained at 20 ± 0.5°C, but similar results were also obtained at 24°C. To count spermatozoa, young adult animals were fixed with 4% paraformaldehyde in PBS for 4 h at 4°C, washed in PBS, postfixed with 0°C methanol for 5 min, and incubated with 100 mM DAPI for 1 h. A *z*-dimension stack of digital fluorescence microscopic images through the spermatheca was generated, and sperm nuclei were counted. Actin filaments were visualized using a modified rhodamine phalloidin staining procedure (Strome, 1986; Rose *et al.*, 1997). Adult hermaphrodite gonads were extruded by decapitation in culture medium (80 mM NaCl, 20 mM KCl, 10 mM $MgCl_2$, 5 mM HEPES, pH 7.2, 10% FBS, 0.01% tetramisole), fixed with 3% paraformaldehyde in PBS containing 0.1% Tween-20 (PBS-TW) for 2 h at room temperature, washed in PBS-TW, and incubated with 0.33 μM rhodamine phalloidin (Molecular Probes, Inc., Eugene, OR) in PBS-TW.

RESULTS

The C. elegans *nid-1 Nidogen Gene*

A single nidogen gene *nid-1* was identified in the *C. elegans* genome in cosmid F54F3 based on sequences generated by the genome sequencing project (Waterston and Sulston, 1995). *nid-1* encodes domains similar to vertebrate nidogen G1, G2, and G3 globular domains and a rod domain of EGF repeats (Figures 1A and 2; Table 1). The region with highest amino acid sequence identity to mammalian nidogen is the G3 domain, particularly the six YWTD repeats of this domain (Springer, 1998). There is also strong similarity in the G2 and G1 domains (Figure 2; Table 1). On the basis of sequence similarity, NID-1 is not significantly more similar to mammalian nidogen-1 than to nidogen-2. However, both NID-1 and nidogen-1 have a carboxyl terminal EGF repeat that is not present in nidogen-2. The major difference between the *C. elegans* and mammalian nidogens is that *nid-1* encodes 12 EGF repeats in the rod domain, whereas vertebrate nidogen-1 and nidogen-2 have four EGF and one or two thyroglobulin repeats in this region. The strongest se-

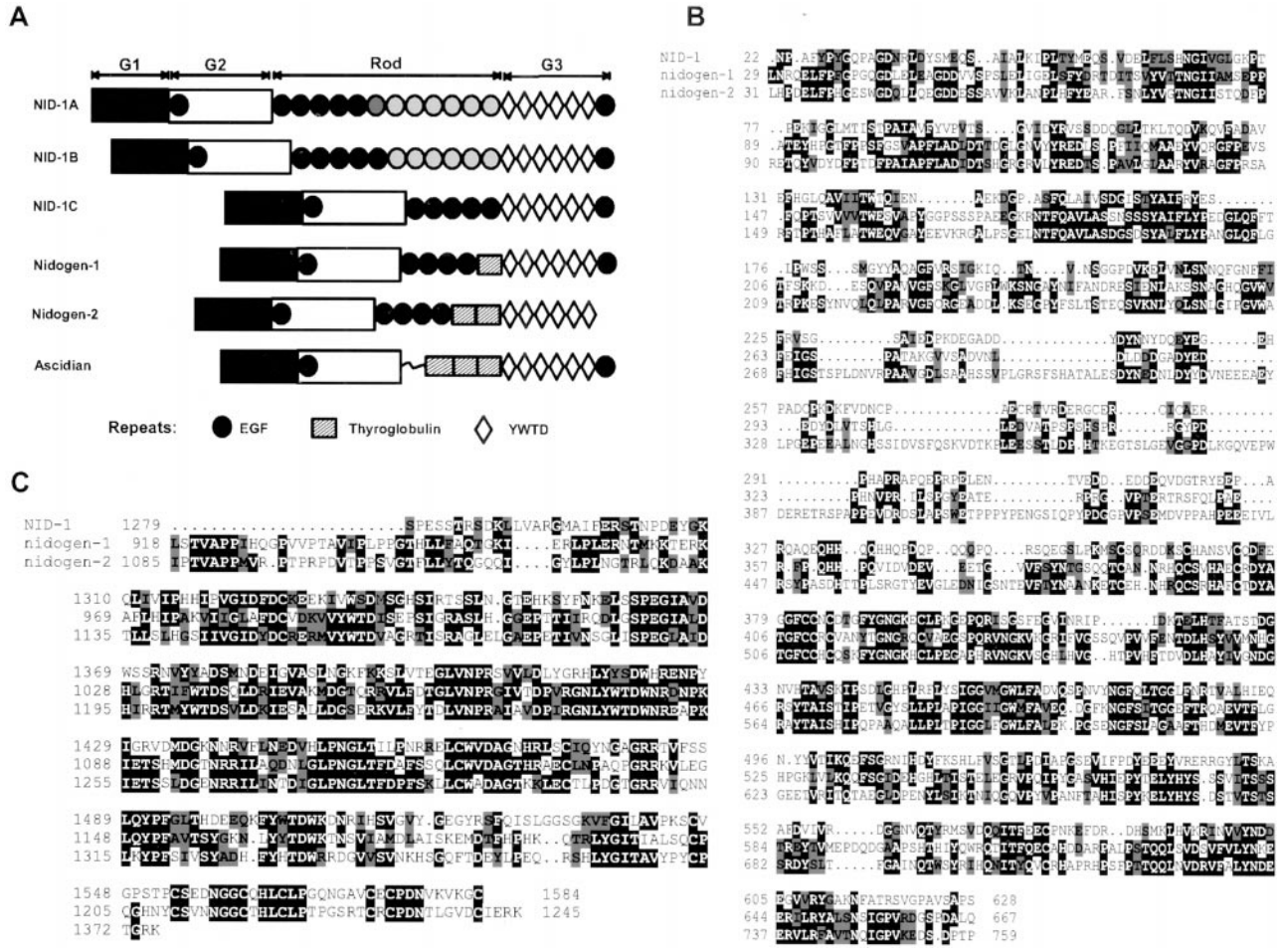

Figure 2. Comparisons of nidogen protein structures and sequences. (A) Domain structures of *C. elegans* NID-1, mouse nidogen-1 (Mann *et al.*, 1989), human nidogen-2 (Kohfeldt *et al.*, 1998), and Ascidian nidogen (Nakae *et al.*, 1993). Domains are represented as follows: ■, G1; □, G2; ○, EGF; ▨, thyroglobulin; ◇, YWTD motif (Springer, 1998). EGF repeats that are present in all forms are colored black, the NID-1A-specific EGF is dark gray, and the NID-1A– and B–specific EGFs are light gray. The extents of domains for NID-1A are indicated at the top. (B) Sequence alignment of the G1 through G2 domains of NID-1, mouse nidogen-1, and human nidogen-2. Identical residues are shown as white letters on black background; similar residues are black letters on gray background. Levels of sequence identity and similarity are presented in Table 1. (C) Sequence alignment of the G3 domains of NID-1, mouse nidogen-1, and human nidogen-2. Residues are highlighted as described for B.

quence conservation has been maintained in the G3 and G2 domains, which mediate binding to laminin and type IV collagen, respectively.

The predicted exon structure of *nid-1* suggested that some of the rod domain EGF repeats could be removed by alternative splicing. We analyzed RT-PCR products and cDNA clones derived from *nid-1* to demonstrate that three isoforms (*nid-1A, B, C*) are generated by alternative splicing (Figures 1 and 2A). All three isoforms contain the amino G1 and G2, and carboxyl G3 globular domains, but they differ in the number of EGF repeats in the rod domain. The longest form, NID-1A, contains all 12 EGF repeats in the rod domain, NID-1B is missing the single EGF repeat encoded by exon 11, and NID-1C lacks 7 EGF repeats encoded by exons 11–14. The NID-1C rod domain, containing five EGF repeats, is most similar in length to mammalian nidogen-1, which has four EGF and one thyroglobulin repeat (Figure 2A).

There is a single RGD (700–702) sequence in mouse nidogen-1, located near the end of the first rod domain EGF repeat. This RGD sequence has been shown to provide a major nidogen cell attachment activity in vitro (Mann *et al.*, 1989; Dong *et al.*, 1995). There is also a single RGD (714–716) present in NID-1, and it is located in the same region of the molecule, at the start of the second rod domain EGF repeat. This RGD sequence is present in all three NID-1 isoforms. There are no RGD sequences in nidogen-2 or the ascidian nidogen.

Expression of nid-1

The *nid-1* isoforms are differentially expressed during development. RNA isolated from embryos contains an abundant transcript of 5.1 kb (Figure 3A). This transcript is approximately the size expected for the *nid-1A* splice isoform, which

Table 1. Amino acid sequence comparisons of *C. elegans* and mammalian nidogens

	Nidogen domains			
	G1–G2[a]	G1	G2	G3
NID-1 vs. nidogen-1	23/34[b]	21/38	29/41	36/49
NID-1 vs. nidogen-2	24/34	26/37	28/38	31/44
nidogen-1 vs. nidogen-2	44/53	44/52	49/61	48/61

[a] The following amino acid residues were utilized for these comparisons: G1–G2: NID-1(22–628), nidogen-1 (29–667), nidogen-2 (31–759); G1: NID-1(22–211), nidogen-1 (29–249), nidogen-2 (31–254). G2: NID-1(348–628), nidogen-1 (375–667), nidogen-2 (472–759). G3: NID-1(1279–1584), nidogen-1 (918–1245), nidogen-2 (1085–1375). The sequences used are mouse nidogen-1 (Mann *et al.*, 1989) and human nidogen-2 (Kohfeldt *et al.*, 1998).

[b] Percentages of amino acid sequence identity and similarity are presented for each comparison as (%identity/%similarity).

is predicted to be 4.8 kb before polyadenylation. The 5.1-kb transcript hybridizes to the form A-specific exon 11, demonstrating that it is the *nid*-1A transcript. No other transcripts are detected when exon 13 or exon 15, which would hybridize to the other isoforms, are used to probe embryo RNA. Transcripts of 5.1 and 4.2 kb are detected in approximately equal abundance in RNA isolated from mixed populations containing animals of all developmental stages (Figure 3A). The 4.2-kb transcript hybridizes to exon 15 but not to exons 11 or 13, indicating that it represents the *nid-1C* isoform (3.8 kb predicted size before polyadenylation).

Probing with exon 13, which would hybridize to *nid-1A* and *nid-1B*, did not reveal any transcripts beyond those detected when exon 11 was used as a probe to visualize the *nid-1A* transcripts. The predicted size of the *nid-1B* transcript (4.6 kb) is only 4% smaller than *nid-1A*, so it may be present in low abundance but masked by the *nid-1A* band. These experiments show that *nid-1A* is the major transcript expressed during embryogenesis and that detectable *nid-1C* expression does not begin until after the completion of embryogenesis.

Specific NID-1 antiserum was raised against a bacterially expressed fusion protein containing the carboxyl-terminal G3 domain that is common to all NID-1 isoforms. Western blots of embryonic *C. elegans* extracts show a strong immunoreactive band migrating at ~170 kDa and a weak band at 160 kDa (Figure 3B). Extracts of mixed stage animals show the 170- and 160-kDa bands as well as a strong band at 150 kDa. The 170- and 150-kDa bands are likely to be NID-1A and C isoforms, because they are similar to the predicted masses of 172 and 136 kDa, respectively, and they exhibit the same temporal characteristics as the *nid-1A* and *nid-1C* transcripts (Figure 3A). The 160-kDa band may be NID-1B, because it is close to the 166-kDa predicted mass for NID-1B. Two or more lower-molecular-weight bands are variably seen in mixed stage extracts and may represent degradation products of NID-1. These results are consistent with the RNA expression data in showing that NID-1A is the major embryonic form and NID-1C is not strongly expressed until after embryogenesis.

NID-1 Tissue Localization

Anti–NID-1 antiserum that reacts with all isoforms was used to localize the protein in whole animals. NID-1 was first detected in embryos at the beginning of morphogenesis (lima stage) localized to body wall muscle cells. As embryos elongate strong NID-1 staining is seen around body wall

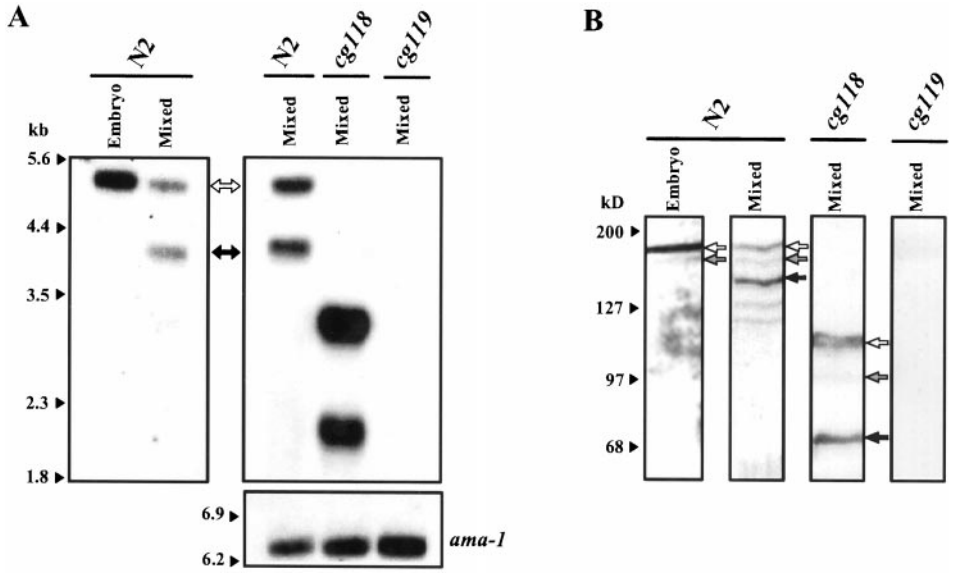

Figure 3. Northern and Western blot analyses of nid-1 expression in wild-type and mutant animals. (A) Detection of *nid-1* transcripts in RNA extracted from wild-type (N2) and *nid-1* mutant (*cg118*, *cg119*) animals. RNAs were extracted from embryos (Embryo) or populations of animals of mixed development stages (Mixed). The positions of *nid-1A* (open arrow) and *nid-1C* (filled arrow) transcripts are indicated between A and B. This blot was probed with radiolabeled *nid-1* exon 15 to reveal all isoforms. Equivalent blots were also probed with exons 11 and 13. Hybridization with the RNA polymerase II gene (*ama-1*) was used as a loading control. The positions of size standards are indicated on the left. (B) Detection of NID-1 in extracts from wild-type (N2) and *nid-1* mutant (*cg118*, *cg119*) animals. Extracts were made from embryos (Embryo) or populations of animals of mixed development stages (Mixed). The positions of putative NID-1A (open arrows), NID-1B (shaded arrows), and NID-C (filled arrows) are indicated to the right of each lane. The positions of molecular weight standards are indicated on the left.

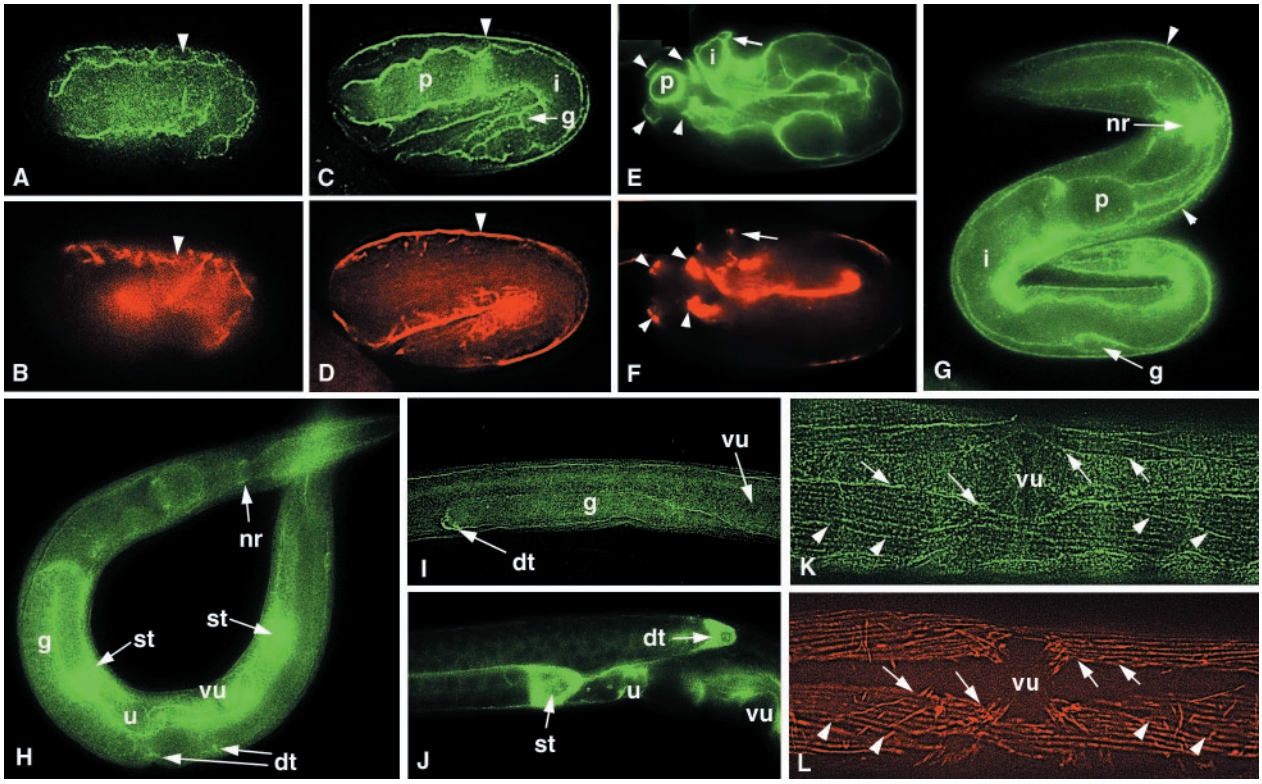

Figure 4. Localization of NID-1 in wild-type animals. Animals were stained with anti–NID-1 (A, C, E, and G–K) and anti-myosin A (B, D, F, and L). (A and B) A comma stage embryo shows strong accumulation of NID-1 around body wall muscle cells (arrowhead) and diffuse association with the pharyngeal and intestinal primordia. (C and D) A twofold stage embryo shows NID-1 accumulation on the basal face of body wall muscles (arrowhead) and on the surfaces of the developing pharynx (p), intestine (i), and gonad (g). (E and F) A threefold stage embryo showing NID-1 localized under the four body wall muscle quadrants (arrowheads) and on the surfaces of the pharynx (p) and intestine (i). A body wall muscle quadrant over the intestine is indicated with an arrow. (G) In an L1 larva, strong NID-1 accumulation is seen around the nerve ring (nr). Staining is also seen at the basal face of body wall muscles (arrowheads) and on the surfaces of the pharynx (p), intestine (i), and gonad (g). (H) In an L4 larva, there is strong NID-1 accumulation on the developing spermathecae (st), vulva (vu), and uterus, and at the distal tip cells (dt). There is also weaker staining on the surfaces of the pharynx and intestine, at the nerve ring (nr), and under body wall muscles. (I) In a late L2-early L3 larva, NID-1 accumulates around the distal tip cell (dt) that is leading growth of the gonad (g). (J) An L4 larva showing strong NID-1 accumulation at the distal tip cell (dt), spermatheca (st), and uterus (u). (K and L) In an adult animal, NID-1 is distributed in a weak punctate pattern under the muscle cell dense bodies and is also present between the muscle quadrants. There is stronger NID-1 accumulation at the edges of the muscle quadrants (arrows) and weak accumulation between adjacent muscle cells (arrowheads). vu, vulva.

muscle cells and diffuse stain begins to accumulate on the surfaces of the pharyngeal and intestinal primordia (Figure 4,A and B). Once the embryo has elongated to the twofold stage, NID-1 has localized to the basal face of the body wall muscles and shows strong accumulation on the surfaces of the pharyngeal, intestinal, and gonad primordia (Figure 4, C and D). In three- and fourfold stage embryos, NID-1 accumulates to higher levels and remains localized under the four body wall muscle quadrants and on the surfaces of the pharynx, intestine, and gonad (Figure 4, E and F). In L1 larvae the intensity of staining of body wall muscle, pharynx, and intestine appears reduced, and strong staining associated with the nerve ring becomes apparent (Figure 4G). This pattern continues through the L2 and L3 larval stages, with the addition of stronger staining of the distal tip cells as they lead the growth of the gonad (Figure 4I). In late L3 to L4 stage larvae particularly strong NID-1 accumulation is seen associated with the distal tip cells and the developing somatic structures of the gonad, the spermatheca, uterus, and vulva (Figure 4, H and J).

Under the body wall muscles of larval and adult stage animals NID-1 is organized as punctate lines (Figure 4, K and L). These lines follow the rows of dense bodies within the muscle cells (Figure 5,A–C). NID-1 also accumulates strongly at the outer edges of the muscle quadrants and more weakly at the boundaries between muscle cells within each quadrant. Less organized NID-1 staining is seen in the regions between the body wall muscle quadrants, presumably associated with the epidermal basement membranes in these regions.

NID-1 accumulates along the four sublateral nerves that run beneath the center of each muscle quadrant (Figure 5, D and E). The sublateral nerves extend along dorso- and ventrolateral tracts from the nerve ring in the anterior of the animal to near the middle of the animal where they turn further lateral to positions coincident with the lateral edges

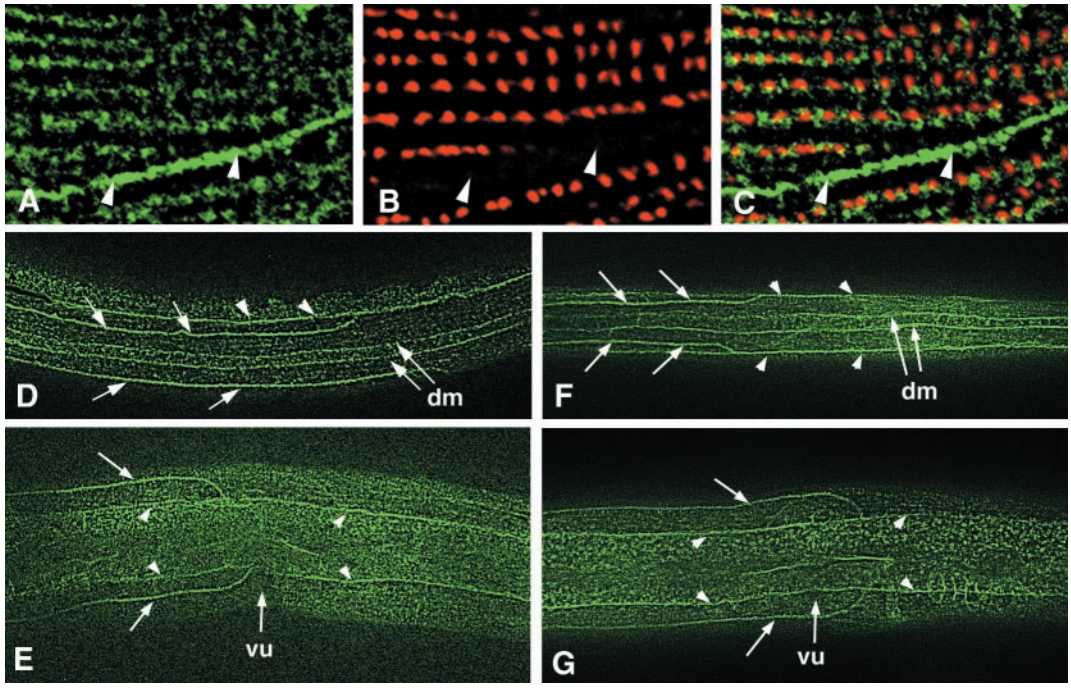

Figure 5. NID-1 localization to sublateral nerves and muscle. Wild-type N2 (A–E) or *nid-1(cg118)* (F and G) animals were stained with anti–NID-1 (A, C–G) or anti–α-actinin (B and C) antibodies. (A–C) Part of a body wall muscle cell of an adult animal costained with anti–NID-1 and anti–α-actinin antibodies. (A) NID-1 accumulates beneath the dense body lines and along the interface between muscle cells (arrowheads). (B) The same region showing anti–α-actinin staining to visualize dense bodies. There is no α-actinin at the muscle cell interface. (C) The merged image of A and B shows that NID-1 localizes along a line that follows the dense bodies. (D and F) Dorsal views of L2 larvae; anterior is to the left. NID-1 is seen to accumulate on the left and right dorsal sublateral nerves (arrows), the dorsal edges of the left and right dorsal muscle quadrants (dm), and the lateral edges of the dorsal muscle quadrants (arrowheads). (E and G) Left lateral views of L4 larvae showing NID-1 accumulation on the dorsal and ventral sublateral nerves (arrows) and along the lateral edges of the dorsal and ventral body wall muscle quadrants (arrowheads). vu, vulvae.

of the body wall muscle quadrants. NID-1 accumulation on these nerves is seen in larval and adult animals and is similar in intensity to the staining at the edges of the body wall muscle quadrants. Staining along the edges of the body wall muscle quadrants appears to be associated with the muscle edges rather than the nerves in these regions because the staining closely follows the edge of the muscles and it does not display the left/right asymmetry expected for the ventral and dorsal nerve cords. As noted above, less organized NID-1 staining is also present in the regions between body wall muscle quadrants.

nid-1 Mutants

A Tc1 transposon insertion was identified near the start of exon 2 in the *nid-1* gene, between the codons for Tyr54 and Met55 (nucleotides 3041–3042). Animals homozygous for the insertion are viable and fertile and display no obvious abnormal phenotypes. The Tc1 element could be removed by RNA splicing and not severely affect *nid-1* function. We therefore identified two deletions caused by imprecise excisions of the Tc1 element. One deletion, *cg118*, removes 2582 nucleotides (3036–5617: GenBank Z79696), resulting in an in-frame fusion of the beginning of exon 2 with part of exon 8 (Figure 1A). This deletion would result in loss of all of the G2 globular domain, part of the G1 domain, and 33 amino acids from the first EGF repeat in the rod domain. The second deletion, *cg119*, removes 3133 nucleotides (1499–4631: GenBank Z79696), extending from 952 nucleotides before the *nid-1* initiator ATG through exon 7 (Figure 1A). After outcrossing to remove extraneous mutations, homozygous *cg118* and *cg119* animals showed no overt abnormal phenotypes.

The effects of both deletions on *nid-1* expression were examined at both the RNA and protein levels. *cg118* animals contain *nid-1* transcripts of ~3.2 and 2.2 kb, ~1.8 kb shorter than in wild type (N2), as predicted by the extent of the deletion (Figure 3A). The truncated *nid-1A* and *C* transcripts are present at approximately wild-type levels. No *nid-1* transcripts are detectable in RNA extracted from *cg119* animals, although control *ama-1* RNA is detected at normal levels in these same samples. Western blots of *cg118* extracts reacted with anti–NID-1 antiserum show strong bands of ~113- and 72-kDa apparent masses and a weak band of 99 kDa (Figure 3B). These sizes are similar to the 103-, 67-, and 97-kDa masses predicted for the *cg118* truncated NID-1A, C, and B products, respectively. The truncated NID-1A and NID-1C proteins are present at approximately wild-type levels. No NID-1 protein is detectable on Western blots of extracts from *cg119* animals reacted with anti–NID-1 antiserum (Figure 3B), and NID-1 is not detectable in these animals by immu-

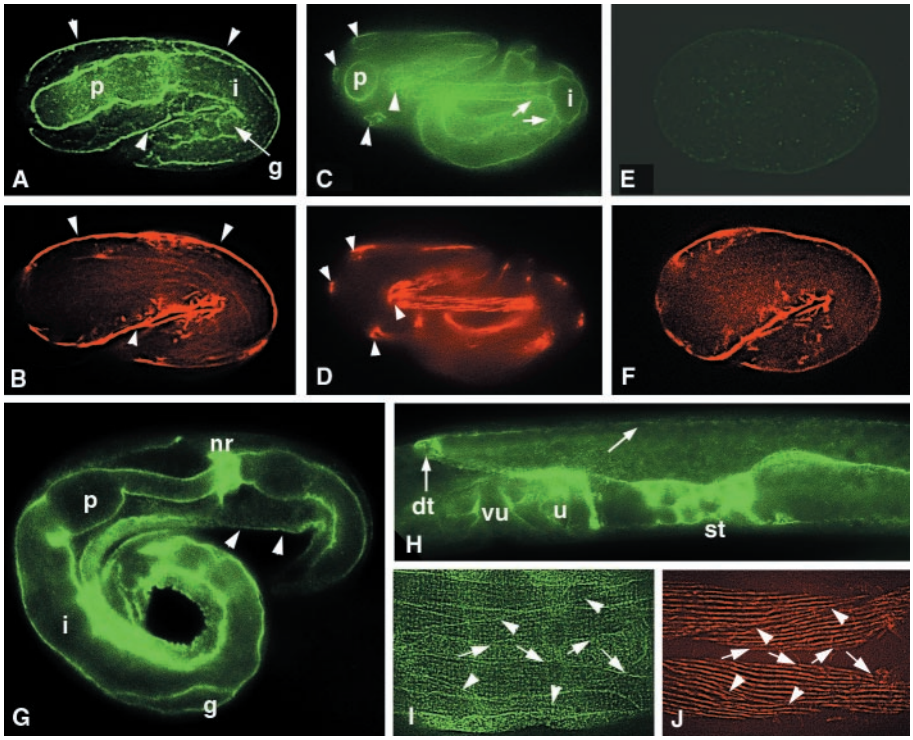

Figure 6. NID-1 localization in *cg118* and *cg119* mutant animals. Animals were stained with anti–NID-1 antiserum (A, C, E, G, H, and I) or anti-myosin A (B, D, F, and J). (A and B) Twofold stage *cg118* mutant embryo shows NID-1 localization under body wall muscle (arrowheads) and on the surfaces of the pharynx (p), intestine (i), and gonad (g). (C and D) Threefold stage *cg118* mutant embryo showing NID-1 accumulation at the basal surfaces (arrowheads) and edges (arrows) of body wall muscle quadrants and on the surfaces of the pharynx (p) and intestine (i). (E and F) Twofold stage *cg119* mutant embryo showing complete lack of staining by anti–NID-1 antibodies. (G) L1 stage *cg118* mutant larva showing NID-1 accumulation at nerve ring (nr), under body wall muscle (arrow), and on the surfaces of the pharynx (p), intestine (i), and gonad (g). (H) Late L4 stage *cg118* mutant larva showing NID-1 accumulation on the developing spermatheca (st), uterus (u), and vulva (vu), and at the distal tip cell (dt). Weaker accumulation on the surface of the gonad is also seen (arrow). (I and J) Ventral view of *cg118* mutant adult hermaphrodite showing NID-1 accumulation at the ventral edges of the ventral body wall muscle quadrants (arrows) and at the edges between adjacent muscle cells (arrowheads).

nofluorescence (Figure 6,E and F). These results show that the *cg119* deletion allele is a molecular null, whereas the *cg118* deletion mutant produces approximately wild-type levels of truncated NID-1 that is missing all of the G2 and part of the G1 domains.

Effect of nid-1(cg118) Deletion on NID-1 Localization

The *cg118* deletion completely removes the G2 domain, which for mouse nidogen-1 has been shown to interact with type IV collagen and perlecan (Reinhardt *et al.*, 1993; Kohfeldt *et al.*, 1998). To determine whether loss of the G2 domain affects the in vivo distribution of nidogen, we performed immunohistochemistry of *cg118* mutant animals with anti–NID-1 antisera (Figure 6). Examination of *cg118* embryos, larvae, and adults revealed no detectable differences from wild-type in the timing of NID-1 appearance, tissue localization, or levels. The *cg118* truncated NID-1 accumulates on the edges of muscle quadrants and on the sublateral nerves in a manner indistinguishable from wild-type NID-1 (Figure 5, F and G). The stability and normal tissue distribution of nidogen are therefore not dependent on the presence of its G2 domain.

Effects of nid-1 Mutations on Type IV Collagen Localization

The ability of mouse nidogen-1 to form a ternary complex between type IV collagen and laminin suggests that it may influence type IV collagen assembly. The wild-type distribution of type IV collagen in *C. elegans* was previously described (Graham *et al.*, 1997). We examined the distribution of type IV collagen in *nid-1* deletion mutant animals using antitype IV collagen antisera (Figure 7). No difference from the wild-type localization pattern was seen in embryos, larvae, or adult homozygotes for either *nid-1* deletion. The fine pattern of collagen IV localization under body wall muscles is not altered in the *nid-1* mutants. We conclude that NID-1 is not required for normal localization of type IV collagen in *C. elegans*.

Effects of nid-1 Mutations on Epithelial Functions

Defects in epithelial morphogenesis and function have been noted when nidogen function has been perturbed in vertebrate cultures of cells or tissues (Ekblom *et al.*, 1994; Kadoya *et al.*, 1997). We examined analogous tissues of *C. elegans* in *cg118* and *cg119* mutant animals. No alterations of the epidermis (hypodermis) were seen using *jam-1*::GFP as a marker to visualize cell–cell junctions. The excretory cell of *C. elegans* is analogous to the vertebrate kidney and extends long tubular processes between the epidermis and the overlying basement membrane (Nelson *et al.*, 1983). These processes appear normal in *nid-1* mutant animals. The gonad is a basement membrane covered tube that forms stereotypical anterior and posterior reflexed arms by directed migrations during development (Kimble and Hirsh, 1979). The gonad migrations occur normally in both *nid-1* mutants. We conclude that nidogen is not required for the proper migrations and organization of these tissues.

Reduced Fecundity of nid-1 Mutants

Although *cg118* and *cg119* mutant strains display no obvious defects in morphology or motility, they do have somewhat

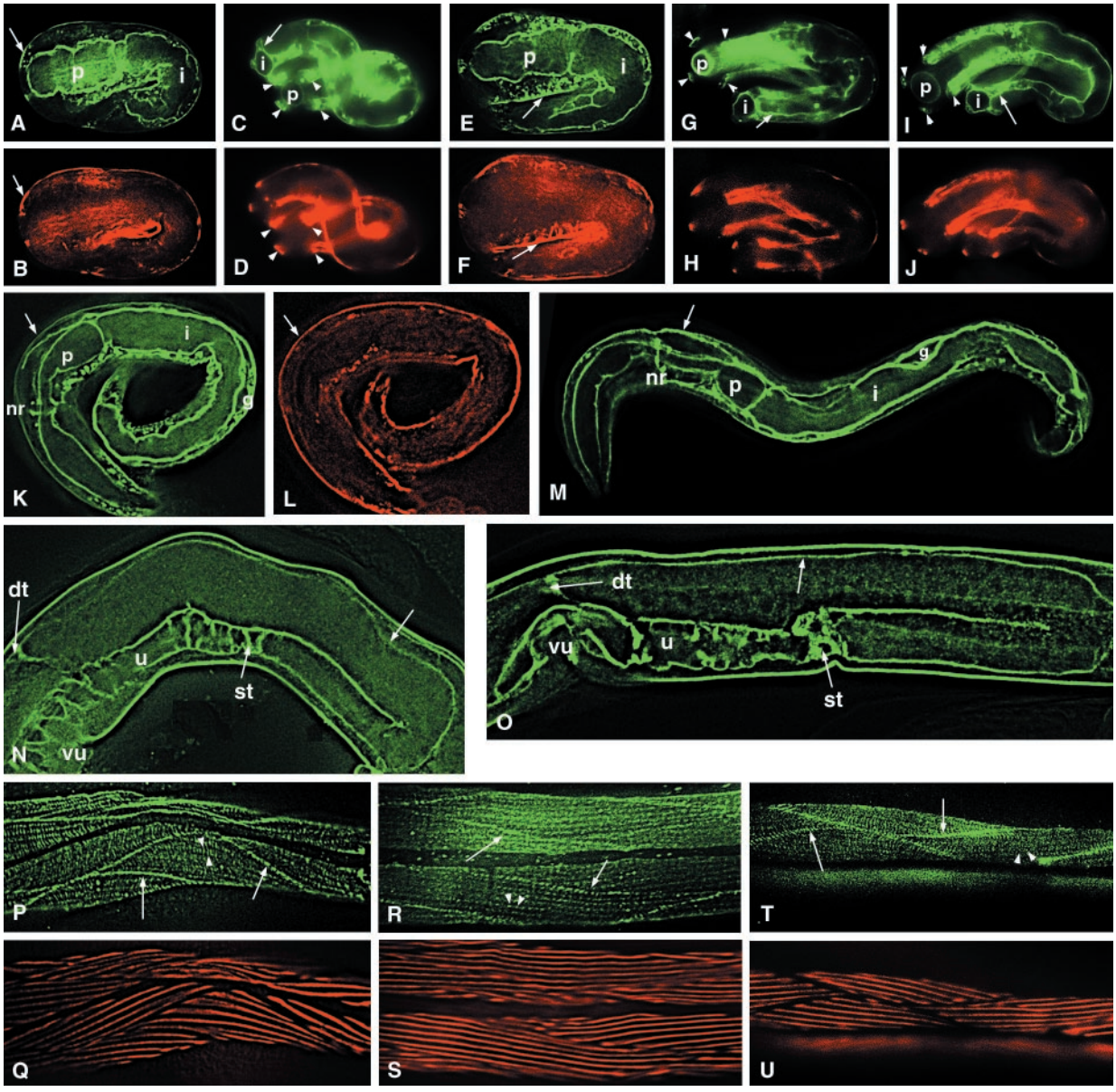

Figure 7. Type IV collagen localization in wild-type and *nid-1* mutant animals. Wild-type N2 (A–D, K, L, N, P, and Q), *cg118* mutant (E–H, M, O, R, and S) or *cg119* mutant (I, J, T, and U) animals were stained with anti–LET-2 type IV collagen antisera (A, C, E, G, I, K, M–P, R, T) or anti-myosin A antibodies (B, D, F, H, J, L, Q, S, and U). (A and B) Wild-type twofold stage embryo showing type IV collagen localization under body wall muscles (arrow) and on the surfaces of the pharynx (p) and intestine (i). (C, D). Wild-type threefold stage embryo showing type IV collagen localization under body wall muscle quadrants (arrowheads), and on the surface of pharynx (p) and intestine (i). (E, F). Twofold stage *cg118* mutant embryo showing type IV collagen localization to body wall muscles (arrow), and on the surfaces of the pharynx (p) and intestine (i). (G and H) Threefold stage *cg118* mutant embryo showing type IV collagen localization under (arrowheads) and at the edges (arrow) of body wall muscle quadrants and on the surfaces of the pharynx (p) and intestine (i). (I and J) Threefold stage *cg119* embryo showing type IV collagen localization under (arrowheads) and at the edges (arrow) of body wall muscle quadrants and on the surfaces of the pharynx (p) and intestine (i). (K and L) Wild-type L1 larva showing type IV collagen localization under body wall muscle (arrow), at the nerve ring (nr), and on the surfaces of the pharynx (p), intestine (i), and gonad (g). (M) L1 stage *cg118* mutant larva shows type IV collagen localization under body wall muscle (arrow), at the nerve ring (nr), and on the surfaces of the pharynx (p), intestine (i), and gonad (g). (N) Wild-type L4 stage larva showing type IV collagen localization to the surface of the gonad (arrow), the distal tip cell (dt), spermatheca (st), and uterus (u). The location of the vulva (vu) is indicated. (O) L4 stage *cg119* mutant larva shows type IV collagen localization to the surface of the gonad (arrow), the distal tip cell (dt), spermatheca (st), and uterus (u). vu, vulva. (P and Q) Wild-type L4 stage larva showing type IV collagen accumulation at the interfaces between muscle cells (arrows) and in a dense body pattern under the cells. (R and S) L4 stage *cg118* mutant animal showing type IV collagen accumulation at the interfaces between muscle cells (arrows) and in a dense body pattern under the cells. (T and U) L4 stage *cg119* mutant animal showing type IV collagen accumulation at the interfaces between muscle cells (arrows) and in a dense body pattern under the cells.

Table 2. Effects of *nid-1* mutations on fecundity

Strain	Eggs laid per animal[a]					% of N2[b]	Sperm per gonad arm[c]	Eggs in uterus[d]
	Day 1	Day 2	Day 3	Day 4	Total			
N2	64 ± 1.8	120 ± 1.8	86 ± 1.5	18 ± 1.5	288 ± 1.0 (n = 50)	100	159 ± 2 (n = 10)	18.9 ± 0.3 (n = 20)
nid-1(cg118)	61 ± 1.7	109 ± 1.5	68 ± 1.5	18 ± 0.6	256 ± 1.8 (n = 50)	89	156 ± 3 (n = 10)	18.4 ± 0.2 (n = 20)
nid-1(cg119)	44 ± 1.1	77 ± 1.9	58 ± 2.1	17 ± 1.0	197 ± 1.7 (n = 50)	68	154 ± 3 (n = 10)	18.1 ± 0.3 (n = 20)

[a] Average number of eggs laid per animal ± SEM.

[b] Total number of eggs laid as a percentage of the wild-type N2 strain.

[c] Average number of sperm per gonad arm ± SEM.

[d] Average number of fertilized eggs in the uterus ± SEM.

reduced fecundity relative to the wild-type N2 strain. On average, *cg119* hermaphrodites have 32% fewer offspring than N2, and *cg118* hermaphrodites have 11% fewer offspring (Table 2). The reduced fecundity of the *nid-1* mutants is not due to reduced numbers of sperm because they contain the same number of sperm in their spermathecae as the N2 strain (Table 2). They do not appear to have an egg-laying defect because they carry the same number of fertilized eggs in the uterus as wild-type animals. There are also no apparent defects in the structure of the spermatheca or uterus observable by Nomarski optics, and rhodamine-phalloidin staining reveals no obvious defects in the actin filaments of the uterus, spermatheca, or sheath cells (data not shown). Although the cause is unclear, the reduced fecundity of *nid-1* mutants would be a substantial selective detriment in the animal's natural environment.

DISCUSSION

Nidogen appears as a major component of basement membranes in all organisms that have been characterized. The ability of nidogen to bind with high affinity to both type IV collagen and laminin suggested that it might be a critical molecule for assembly of basement membranes. In vitro studies in vertebrate systems have supported the potential importance of nidogen for cell adhesion and tissue morphogenesis. We have shown that loss of nidogen in *C. elegans* results in viable animals that are fertile and that display no overt abnormal phenotypes. Loss of other *C. elegans* basement membrane components, such as type IV collagen (Guo *et al.*, 1991; Sibley *et al.*, 1993; Gupta *et al.*, 1997), perlecan (Rogalski *et al.*, 1993), or SPARC (Fitzgerald and Schwarzbauer, 1998), results in embryonic lethality. If nidogen were critical for the assembly or function of these constituents of basement membranes, then its absence would also be expected to result in lethality. The fact that this is not the case provides strong evidence that nidogen is not required for these molecules to assemble into functional basement membranes.

nid-1 is the only gene in *C. elegans* that encodes a classical nidogen with G1, G2, rod, and G3 domains. There are, however, other genes that encode nidogen-related domains. Three predicted gene products (B0393.5, D1044.2, K03H1.5) contain G1-like domains. All three also encode predicted transmembrane domains near their carboxyl-termini, suggesting that they are cell surface transmembrane proteins. Six distinct predicted gene products contain YWTD motifs related to the nidogen G3 domain: five are predicted to be transmembrane, one is predicted to be secreted. All six also contain EGF repeats but no other similarities to nidogen. There are no other genes that encode nidogen G2–related domains. It is possible that the nidogen G1– and/or G3–related domains of these other gene products could replace NID-1 functions in *nid-1* mutant animals.

Our immunolocalization studies show that NID-1 accumulates at all sites where type IV collagen was previously shown to assemble (Graham *et al.*, 1997) but is additionally found at sites where little or no collagen IV is detected. In particular, NID-1 shows strong accumulation around the nerve ring, whereas collagen IV is only weakly detected in this region. NID-1 accumulates on the sublateral nerves, where collagen IV shows no preferential accumulation. Both collagen IV and nidogen show strong accumulation under body wall muscles during embryonic development, but the level of nidogen decreases during larval and adult stages, whereas collagen IV levels are maintained. Nidogen accumulates strongly at the edges of the muscle quadrants and only weakly at the junctions between adjacent muscle cells, whereas collagen IV shows the opposite pattern, being strongest at muscle cell junctions. NID-1 also shows diffuse accumulation on the regions of the epidermal basement membrane that lie between the body wall muscle quadrants, whereas collagen IV is absent from these regions. Thus, although collagen IV and nidogen are generally coincident, there are sites where substantial differences in their relative abundance are seen. These results indicate that there is not a one-to-one correspondence between collagen IV and nidogen in *C. elegans* basement membranes.

Type IV collagen assembles into all basement membranes of *C. elegans* except on the regions of the epidermis that are located between the body wall muscle quadrants and on the pseudocoelomic faces of the muscle quadrants (Graham *et al.*, 1997). We had expected that nidogen would be involved in localization of collagen IV assembly, based on its ability to link collagen IV and laminin. However, we showed that type IV collagen assembles in a completely normal manner in the absence of nidogen. How is assembly of type IV collagen restricted to particular locations? Type IV collagen could be localized to cell surfaces by binding to integrins. However, in mutants for two *C. elegans* integrins, *ina-1* α-integrin

(Baum and Garriga, 1997) and *pat-3* β-integrin (Gettner *et al.*, 1995), type IV collagen localization appears normal (J. Kramer, unpublished results). It is possible that collagen IV assembly is dependent on other integrins or some other unidentified molecule. It is also possible that there are redundant mechanisms for collagen IV localization, such that loss of any one binding molecule will not reveal abnormalities in collagen assembly.

The mammalian nidogen-1 G2 domain binds type IV collagen and perlecan with high affinity (Reinhardt *et al.*, 1993). The *C. elegans* and mammalian G2 domains show strong sequence conservation, suggesting that the *C. elegans* G2 domain is likely to also be capable of binding collagen IV and perlecan. The *nid-1(cg118)* deletion completely removes the nidogen G2 domain as well as parts of G1 and the first EGF repeat of the rod domain. The *cg118*-deleted NID-1 accumulates to approximately normal levels and shows normal tissue localization. Thus, the G2 domain has little or no role in nidogen stability or assembly into basement membranes. Nidogen localization therefore appears to occur independently of collagen IV and perlecan interactions.

If linking between collagen IV and laminin were a critical aspect of nidogen function, then the *cg118* G2 domain deletion might be expected to act as a dominant interfering mutant. The truncated NID-1 could bind to laminin but would be unable to bind type IV collagen. Mammalian nidogen-1 was found to cooperate with laminin-1 to stimulate β-casein synthesis by cultured mammary epithelial cells (Pujuguet *et al.*, 2000). However, addition of the nidogen-1 G3 domain inhibited laminin-1 stimulation of β-casein synthesis, suggesting that the presence of the laminin-binding G3 domain in the absence of other parts of nidogen dominantly interferes with laminin signaling. In coculture studies, antisense inhibition of laminin expression blocked the accumulation of type IV collagen and nidogen at the epithelial/mesenchymal interface (De Arcangelis *et al.*, 1996), leading to the suggestion that linkage of collagen IV to laminin via nidogen was essential for its assembly. The fact that the *cg118* G2 deletion nidogen does not cause dominant phenotypes indicates that its binding to laminin does not interfere with any essential processes. If nidogen was required to link type IV collagen to laminin, then the *cg118* deletion NID-1 should dominantly interfere with this process.

We have identified three alternative splice isoforms of NID-1 that contain differing numbers of EGF repeats in their rod domains. NID-1A is the longest and is the predominant embryonic form, whereas the shortest, NID-1C, only appears after the completion of embryogenesis. The different numbers of EGF repeats would change the spacing between the collagen IV and laminin-binding domains of the NID-1 isoforms and could also change their binding repertoires. Alternative splice forms of other nidogen genes have not been reported. However, mammals have two nidogen genes that may provide additional diversity of nidogen function.

The alternative splice isoforms of *nid-1* are reminiscent of *let-2*, the α2(IV) collagen gene of *C. elegans*. *let-2* generates two alternative splice isoforms that dramatically change relative abundance immediately after the completion of embryogenesis (Sibley *et al.*, 1993). The *C. elegans* perlecan gene *unc-52* also produces alternatively spliced variants that differ in their expression during development (Mullen *et al.*, 1999). The basement membranes of *C. elegans* appear to undergo significant changes in composition on completion of embryogenesis.

Perturbation of nidogen-1 function in cultured mammalian kidney, lung, or submandibular gland (Ekblom *et al.*, 1994; Kadoya *et al.*, 1997) and correlation of nidogen proteolysis with mammary gland involution (Alexander *et al.*, 1996) have suggested that nidogen has important roles in epithelial function. We particularly looked in *C. elegans nid-1* mutants at tissues that would reveal defects in epithelial morphogenesis. In *nid-1* mutants no defects were seen in the excretory canals, which are analogous to the vertebrate kidney, the gonad, which forms by directed migration of a basement membrane enclosed tube, or in organization of the hypodermal cells, which form the epidermis of nematodes. We conclude that nidogen is not required for morphogenesis of these epithelia in *C. elegans*. It is possible that such functions for nidogen have arisen in vertebrates or that the in vitro studies are misleading as to the in vivo functions of nidogen.

We showed that *nid-1* mutations cause reduced fecundity. The *nid-1* null mutant showed a greater reduction (32%) than the G2 domain deletion mutant (11%). Thus, NID-1 lacking the G2 domain is able to provide some, but not all, of the nidogen function required for normal fecundity. The cause of the reduced fecundity of *nid-1* mutants has not been elucidated. However, NID-1 shows strong accumulation around the developing spermatheca, uterus, and vulva. Although no defects were detected in these structures, it is possible that they do not function optimally in the absence of nidogen. The reduced fecundity that results from either of these *nid-1* mutations would result in sufficient selective pressure to ensure maintenance of the gene, even in the absence of any other functions.

During preparation of this article a report appeared showing that a *nid-1* mutation, *ur41*, can affect positioning of longitudinal nerves in *C. elegans* (Kim and Wadsworth, 2000). The *nid-1(ur41)* mutation results in no overt morphological or behavioral phenotypes, in agreement with our findings. The nerve positioning defects are only detectable using GFP markers to visualize the affected axons. The most penetrant defect reported was mispositioning of the dorsal sublateral nerves up toward the dorsal midline. Our demonstration that NID-1 accumulates on the sublateral nerves indicates that it directly associates with the affected axons. The strong accumulation of NID-1 at the edges of the body wall muscle quadrants that we demonstrated is consistent with the proposal that nidogen may influence the guidance decisions of dorsoventrally migrating axons at the interfaces between muscle and epidermis (Kim and Wadsworth, 2000).

ACKNOWLEDGMENTS

We thank Dr. J. Culotti for identifying the *nid-1(ev608)* allele, Dr. J. Hardin for *jcIs1*, Dr. Y. Kohara for cDNA clones, and A. Coulson for cosmids. Some strains used in these studies were provided by the *Caenorhabditis elegans* Genetics Center, which is supported by the National Institutes of Health Center for Research Resources. This work was supported by National Institutes of Health grant HD-27211, to J.M.K.

REFERENCES

Alexander, C.M., Howard, E.W., Bissell, M.J., and Werb, Z. (1996). Rescue of mammary epithelial cell apoptosis and entactin degrada-

tion by a tissue inhibitor of metalloproteinases-1 transgene. J. Cell Biol. *135*, 1669–1677.

Aumailley, M., Battaglia, C., Mayer, U., Reinhardt, D., Nischt, R., Timpl, R., and Fox, J.W. (1993). Nidogen mediates the formation of ternary complexes of basement membrane components. Kidney Int. *43*, 7–12.

Baum, P.D., and Garriga, G. (1997). Neuronal migrations and axon fasciculation are disrupted in *ina-1* integrin mutants. Neuron *19*, 51–62.

Brenner, S. (1974). The genetics of *Caenorhabditis elegans*. Genetics *77*, 71–94.

Chung, A.E., Dong, L.J., Wu, C.Y., and Durkin, M.E. (1993). Biological functions of entactin. Kidney Int. *43*, 13–19.

De Arcangelis, A., Neuville, P., Boukamel, R., Lefebvre, O., Kedinger, M., and Simon-Assmann, P. (1996). Inhibition of laminin alpha 1-chain expression leads to alteration of basement membrane assembly and cell differentiation. J. Cell Biol. *133*, 417–430.

Dong, L.J., Hsieh, J.C., and Chung, A.E. (1995). Two distinct cell attachment sites in entactin are revealed by amino acid substitutions and deletion of the RGD sequence in the cysteine-rich epidermal growth factor repeat 2. J. Biol. Chem. *270*, 15838–15843.

Durkin, M.E., Chakravarti, S., Bartos, B.B., Liu, S.H., Friedman, R.L., and Chung, A.E. (1988). Amino acid sequence and domain structure of entactin. Homology with epidermal growth factor precursor and low density lipoprotein receptor. J. Cell Biol. *107*, 2749–2756.

Dziadek, M., and Timpl, R. (1985). Expression of nidogen and laminin in basement membranes during mouse embryogenesis and in teratocarcinoma cells. Dev. Biol. *111*, 372–382.

Ekblom, P., Ekblom, M., Fecker, L., Klein, G., Zhang, H.Y., Kadoya, Y., Chu, M.L., Mayer, U., and Timpl, R. (1994). Role of mesenchymal nidogen for epithelial morphogenesis in vitro. Development *120*, 2003–2014.

Finney, M., and Ruvkun, G.B. (1990). The *unc-86* gene product couples cell lineage and cell identity in *C. elegans.* Cell *63*, 895–905.

Fitzgerald, M.C., and Schwarzbauer, J.E. (1998). Importance of the basement membrane protein SPARC for viability and fertility in *Caenorhabditis elegans*. Curr. Biol. *8*, 1285–1288.

Form, D.M., Pratt, B.M., and Madri, J.A. (1986). Endothelial cell proliferation during angiogenesis. Lab. Invest. *55*, 521–530.

Fox, J.W., Mayer, U., Nischt, R., Aumailley, M., Reinhardt, D., Wiedemann, H., Mann, K., Timpl, R., Krieg, T., Engel, J., et al. (1991). Recombinant nidogen consists of three globular domains and mediates binding of laminin to collagen type IV. EMBO J. *10*, 3137–3146.

Francis, G.R., and Waterston, R.H. (1985). Muscle organization in *Caenorhabditis elegans*: localization of proteins implicated in thin filament attachment and I-band organization. J. Cell Biol. *101*, 1532–1549.

Gettner, S.N., Kenyon, C., and Reichardt, L.F. (1995). Characterization of beta pat-3 heterodimers, a family of essential integrin receptors in *C. elegans.* J. Cell Biol. *129*, 1127–1141.

Graham, P.L., Johnson, J.J., Wang, S.R., Sibley, M.H., Gupta, M.C., and Kramer, J.M. (1997). Type IV collagen is detectable in most, but not all, basement membranes of *Caenorhabditis elegans* and assembles on tissues that do not express it. J. Cell Biol. *137*, 1171–1183.

Guo, X., Johnson, J.J., and Kramer, J.M. (1991). Embryonic lethality caused by mutations in basement membrane collagen of *C. elegans.* Nature *349*, 707–709.

Gupta, M.C., Graham, P.L., and Kramer, J.M. (1997). Characterization of alpha 1(IV) collagen mutations in *Caenorhabditis elegans* and the effects of alpha 1 and alpha 2(IV) mutations on type IV collagen distribution. J. Cell Biol. *137*, 1185–1196.

Kadoya, Y., Salmivirta, K., Talts, J.F., Kadoya, K., Mayer, U., Timpl, R., and Ekblom, P. (1997). Importance of nidogen binding to laminin gamma 1 for branching epithelial morphogenesis of the submandibular gland. Development *124*, 683–691.

Kim, S., and Wadsworth, W.G. (2000). Positioning of longitudinal nerves in *C. elegans* by nidogen. Science *288*, 150–154.

Kimble, J., and Hirsh, D. (1979). The postembryonic cell lineages of the hermaphrodite and male gonads in *Caenorhabditis elegans.* Dev. Biol. *70*, 396–417.

Kohfeldt, E., Sasaki, T., Göhring, W., and Timpl, R. (1998). Nidogen-2: a new basement membrane protein with diverse binding properties. J. Mol. Biol. *282*, 99–109.

Kramer, J.M. (1997). Extracellular matrix structure and function. In: The Nematode *C. elegans* II, ed. D. L. Riddle, Cold Spring Harbor, NY: Cold Spring Harbor Laboratory, 471–500.

Kuschegullberg, M., Garrison, K., Mackrell, A.J., Fessler, L.I., and Fessler, J.H. (1992). Laminin-A chain-expression during *Drosophila* development and genomic sequence. EMBO J. *11*, 4519–4527.

Leivo, I., Vaheri, A., Timpl, R., and Wartiovaara, J. (1980). Appearance and distribution of collagens and laminin in the early mouse embryo. Dev. Biol. *76*, 100–114.

Mann, K., Deutzmann, R., Aumailley, M., Timpl, R., Raimondi, L., Yamada, Y., Pan, T., Conway, D., and Chu, M.-L. (1989). Amino acid sequence of mouse nidogen, a multidomain basement membrane protein with binding activity for laminin, collagen IV and cells. EMBO J. *8*, 65–72.

Mayer, U., Nischt, R., Poschl, E., Mann, K., Fukuda, K., Gerl, M., Yamada, Y., and Timpl, R. (1993). A single EGF-like motif of laminin is responsible for high affinity nidogen binding. EMBO J. *12*, 1879–1885.

Moerman, D.G., Hutter, H., Mullen, G.P., and Schnabel, R. (1996). Cell autonomous expression of perlecan and plasticity of cell shape in embryonic muscle of *Caenorhabditis elegans.* Dev. Biol. *173*, 228–242.

Mohler, W.A., Simske, J.S., Williams-Masson, E.M., Hardin, J.D., and White, J.G. (1998). Dynamics and ultrastructure of developmental cell fusions in the *Caenorhabditis elegans* hypodermis. Curr. Biol. *8*, 1087–1090.

Mullen, G.P., Rogalski, T.M., Bush, J.A., Gorji, P.R., and Moerman, D.G. (1999). Complex patterns of alternative splicing mediate the spatial and temporal distribution of perlecan/UNC-52 in *Caenorhabditis elegans.* Mol. Biol. Cell *10*, 3205–3221.

Nakae, H., Sugano, M., Ishimori, Y., Endo, T., and Obinata, T. (1993). Ascidian entactin/nidogen implication of evolution by shuffling 2 kinds of cysteine-rich motifs. Eur. J. Biochem. *213*, 11–19.

Nelson, F.K., Albert, P.S., and Riddle, D.L. (1983). Fine structure of the *Caenorhabditis elegans* secretory-excretory system. J. Ultrastruct. Res. *82*, 156–171.

Plasterk, R.H.A. (1995). Reverse genetics: from gene sequence to mutant worm. In: Methods in Cell Biology, Vol. 48, ed. H. F. Epstein, and D. C. Shakes, San Diego: Academic Press Inc., 59–80.

Pujuguet, P., Simian, M., Liaw, J., Timpl, R., Werb, Z., and Bissell, M.J. (2000). Nidogen-1 regulates laminin-1-dependent mammary-specific gene expression. J. Cell Sci. *113*, 849–858.

Reinhardt, D., Mann, K., Nischt, R., Fox, J.W., Chu, M.L., Krieg, T., and Timpl, R. (1993). Mapping of nidogen binding sites for collagen type-IV, heparan sulfate proteoglycan, and zinc. J. Biol. Chem. *268*, 10881–10887.

Rogalski, T.M., Williams, B.D., Mullen, G.P., and Moerman, D.G. (1993). Products of the *unc-52* gene in *Caenorhabditis elegans* are homologous to the core protein of the mammalian basement membrane heparan sulfate proteoglycan. Genes Dev. *7*, 1471–1484.

Rose, K.L., Winfrey, V.P., Hoffman, L.H., Hall, D.H., Furuta, T., and Greenstein, D. (1997). The POU gene ceh-18 promotes gonadal sheath cell differentiation and function required for meiotic maturation and ovulation in *Caenorhabditis elegans*. Dev. Biol. *192*, 59–77.

Sambrook, J., Fritsch, E.F., and Maniatis, T. (1989). Molecular Cloning, Cold Spring Harbor, NY; Cold Spring Harbor Laboratory Press.

Sibley, M.H., Johnson, J.J., Mello, C.C., and Kramer, J.M. (1993). Genetic identification, sequence, and alternative splicing of the *Caenorhabditis elegans* α2(IV) collagen gene. J. Cell Biol. *123*, 255–264.

Springer, T.A. (1998). An extracellular beta-propeller module predicted in lipoprotein and scavenger receptors, tyrosine kinases, epidermal growth factor precursor, and extracellular matrix components. J. Mol. Biol. *283*, 837–862.

Strome, S. (1986). Fluorescence visualization of the distribution of microfilaments in gonads and early embryos of the nematode *Caenorhabditis elegans.* J. Cell Biol. *103,* 2241–2252.

Talts, J.F., Andac, Z., Gohring, W., Brancaccio, A., and Timpl, R. (1999). Binding of the G domains of laminin alpha 1 and alpha 2 chains and perlecan to heparin, sulfatides, alpha-dystroglycan and several extracellular matrix proteins. EMBO J. *18*, 863–870.

Timpl, R. (1996). Macromolecular organization of basement membranes. Curr. Opin. Cell Biol. *8*, 618–624.

Waterston, R., and Sulston, J. (1995). The genome of *Caenorhabditis elegans.* Proc. Natl. Acad. Sci. USA *92,* 10836–10840.

Wu, C.Y., Chung, A.E., and McDonald, J.A. (1995). A novel role for alpha 3 beta 1 integrins in extracellular matrix assembly. J. Cell Sci. *108*, 2511–2523.

Yelian, F.D., Edgeworth, N.A., Dong, L.J., Chung, A.E., and Armant, D.R. (1993). Recombinant entactin promotes mouse primary trophoblast cell adhesion and migration through the arg-gly-asp (RGD) recognition sequence. J. Cell Biol. *121*, 923–929.

Yurchenco, P.D. (1994). Assembly of laminin and type-IV collagen into basement membrane networks. In: Extracellular Matrix Assembly and Structure (Biology of Extracellular Matrix Series), ed. P. D. Yurchenco, D. E. Birk, and R. P. Mecham, San Diego: Academic Press Inc, 351–388.

Yurchenco, P.D., and Cheng, Y.S. (1993). Self-assembly and calcium-binding sites in laminin-A 3-arm interaction model. J. Biol. Chem. *268*, 17286–17299.

Yurchenco, P.D., Cheng, Y.S., and Colognato, H. (1992). Laminin forms an independent network in basement membranes. J. Cell Biol. *117*, 1119–1133.

Yurchenco, P.D., and Furthmayr, H. (1984). Assembly of basement membrane collagen. Biochemistry *23,* 1839–1850.